

## Epitaxial integration of $\text{CoFe}_2\text{O}_4$ thin films on Si (001) surfaces using TiN buffer layers

Pilar Prieto<sup>1</sup>, José F. Marco<sup>2</sup>, José E. Prieto<sup>3</sup>, Sandra Ruiz-Gomez<sup>4</sup>, Lucas Perez<sup>4,5</sup>, Rafael P. del Real<sup>6</sup>, Manuel Vázquez<sup>6</sup> and Juan de la Figuera<sup>2</sup>

<sup>1</sup> Dpto. Física Aplicada M-12, Universidad Autónoma de Madrid, 28049 Madrid, Spain

<sup>2</sup> Instituto de Química Física “Rocasolano”, CSIC, 28006 Madrid, Spain

<sup>3</sup> Centro de Microanálisis de Materiales (CMAM) and Dpto. Física de la Materia Condensada, Universidad Autónoma de Madrid, 28049 Madrid, Spain.

<sup>4</sup> Dpto. de Física de Materiales and Unidad Asociada IQFR-CSIC, Universidad Complutense de Madrid, Madrid E-28040, Spain

<sup>5</sup> IMDEA Nanoscience, 28049 Madrid, Spain

<sup>6</sup> Instituto de Ciencia de Materiales de Madrid, CSIC, E-28049 Madrid, Spain

Epitaxial cobalt ferrite thin films with strong in-plane magnetic anisotropy have been grown on Si (001) substrates using a TiN buffer layer. The epitaxial films have been grown by ion beam sputtering using either metallic,  $\text{CoFe}_2$ , or ceramic,  $\text{CoFe}_2\text{O}_4$ , targets. X-ray diffraction (XRD) and Rutherford spectroscopy (RBS) in random and channeling configuration have been used to determine the epitaxial relationship  $\text{CoFe}_2\text{O}_4$  [100] / TiN [100] / Si [100]. Mössbauer spectroscopy, in combination with XRD and RBS, has been used to determine the composition and structure of the cobalt ferrite thin films. The TiN buffer layer induces a compressive strain in the cobalt ferrite thin films giving rise to an in-plane magnetic anisotropy. The degree of in-plane anisotropy depends on the lattice mismatch between  $\text{CoFe}_2\text{O}_4$  and TiN, which is larger for  $\text{CoFe}_2\text{O}_4$  thin films grown on the reactive sputtering process with ceramic targets.

Corresponding author:

e-mail: pilar.prieto@uam.es; fax: +34 91 4973969; tel: +34 91 4975265

**KEYWORDS:** Cobalt ferrite, epitaxial thin films, silicon device integration, magnetic anisotropy.

## 1. Introduction

$\text{CoFe}_2\text{O}_4$  (CFO) is a promising ferromagnetic tunnel barrier material that can be used as a spin filter to create a spin-polarized current [1]. A high electrical resistance and room temperature ferrimagnetism are among its attractive properties. It is also a common material of choice in magnetic recording media. Furthermore, it serves as a magnetic component of read/write heads [2] as well as in other magneto-optic applications [3]. Below the Curie temperature (860 K),  $\text{CoFe}_2\text{O}_4$  has magnetic easy axis along  $\langle 100 \rangle$  directions with a high saturation magnetization,  $400 \text{ emu/cm}^3$ , and a magnetocrystalline anisotropy constant of  $2 \times 10^5 \text{ J/m}^3$  which is an order of magnitude greater than other spinel structure ferrites, resulting in a high coercivity,  $\approx 3000 \text{ Oe}$  [4, 5].  $\text{CoFe}_2\text{O}_4$  has also been investigated for its magnetoelastic properties. Due to its large magnetostriction,  $\text{CoFe}_2\text{O}_4$  has been chosen to build strain driven multiferroic nanostructures [6]. For many of these applications, highly oriented growth of ferrite films is necessary.

The magnetic and electronic properties of  $\text{CoFe}_2\text{O}_4$  are strongly influenced by its cationic arrangement [7-9]. In the spinel ferrites the anions form a face-centered cubic structure (fcc). The structure contains two types of interstitial sites with tetrahedral (A-site) and octahedral (B-site) oxygen coordination. The canonical formula for the completely inverse spinel cobalt ferrite is  $(\text{Fe}^{3+})_A(\text{Co}^{2+}\text{Fe}^{3+})_B\text{O}_4$ , but the particular cation distribution in real samples can differ from that one. Usually CFO has a fraction of divalent  $\text{Co}^{2+}$  ions in tetrahedral sites and the inversion degree  $\gamma$ , defined as the fraction of divalent ions in octahedral sites, is lower than 1. The presence of  $\text{Co}^{2+}$  ions at tetrahedral sites induces changes in the magnetic and electronic properties. In canonical CFO the  $\text{Fe}_A^{3+}$  and  $\text{Fe}_B^{3+}$  are coupled antiferromagnetically and their spin magnetic moments cancel, so the magnetic moment is due mostly to the octahedral  $\text{Co}^{2+}$  cations. The unquenched orbital moment of  $\text{Co}^{2+}$  cations in the crystalline field of octahedral sites is the cause of the large magnetocrystalline anisotropy of CFO [10].

The magnetic behavior of  $\text{CoFe}_2\text{O}_4$  epitaxial thin films is also often different from that of the bulk due to the presence of structural defects that appear during growth, i.e antiphase boundaries, and to strain effects. A common issue in  $\text{CoFe}_2\text{O}_4$  thin films is a significant reduction of the magnetic moment respect to the bulk one when it grows epitaxially on different substrates. The magnetic anisotropy is also strongly affected by the substrate and the defects induced during the epitaxial growth.  $\text{CoFe}_2\text{O}_4$  thin films grow epitaxially on  $\text{MgO}$ ,  $\text{MgAl}_2\text{O}_4$  and  $\text{SrTiO}_3$  substrates [11-21], despite the lattice mismatch of -0.3%, 3.7% and 7.5% between CFO and  $\text{MgO}$ ,  $\text{MgAl}_2\text{O}_4$  and  $\text{SrTiO}_3$  substrates, respectively. In general, the in-plane compressive strain induced by  $\text{MgAl}_2\text{O}_4$  and  $\text{SrTiO}_3$  substrates produce in-plane magnetic anisotropy [11,14,19-21] while perpendicular magnetic anisotropy is induced by  $\text{MgO}$  substrates [11,12].

The incorporation of spinel oxides as active materials in electronics will depend on their integration with silicon wafers having properties comparable to the  $\text{CoFe}_2\text{O}_4$

films grown on oxide single-crystal substrates. The use of controlled buffer layers, that minimize chemical interactions with the silicon substrate and induce domain matching epitaxy [22], is a requisite for this integration. In domain matching epitaxy the misfit between two layers is accommodated by a different number of planes of each layer with a low overall strain. MgO has been used as a buffer layer to grow epitaxially  $\text{CoFe}_2\text{O}_4$  on Si (001) substrates [23]. However Mg inter-diffuses into the  $\text{CoFe}_2\text{O}_4$  thin films at the high temperatures required for good quality growth [24,25]. Yttria-stabilized zirconia (YSZ) template layers or double  $\text{CeO}_2$ /YSZ buffer layers also provide a good platform to integrate  $\text{CoFe}_2\text{O}_4$  with silicon (001) [26,27]. For the integration on Si (111) wafers, buffer layers of  $\text{Sc}_2\text{O}_3$  have also explored [28]. The use of buffer layers has also been used to switch the magnetic anisotropy of  $\text{CoFe}_2\text{O}_4$  films on  $\text{SrTiO}_3$  substrates [29].

TiN is also a good candidate to promote epitaxial growth on silicon substrates. The epitaxial growth of TiN thin films on silicon substrates is well known on semiconductor devices for the fabrication of direct ohmic contacts as well as for diffusion barriers. TiN thin films have the advantage of showing metallic character, presenting good stability at high temperatures, are mechanically robust, and have been used as top and bottom electrodes for RAM capacitors [22]. However the  $\approx 22\%$  lattice misfit between TiN and Si (001) forces some type of strain relaxation at their interface and the epitaxial growth is possible through domain matching epitaxy [30]. The epitaxial growth is possible in the so-called 5-on-4 cube-on-cube bulk superstructure where 5 unit cells of TiN (0.424nm) sit on 4 unit cells of Si (0.543 nm). Depending on the TiN deposition conditions, sometimes a 4-on-3 cube-on-cube growth has been observed [30-32]. In both cases, the resulting overall mismatch of the TiN on Si (001) is -2.4% and 4% respectively. We have recently demonstrated that it is possible to obtain epitaxial and oriented  $\text{Fe}_3\text{O}_4$  thin films, through a TiN buffer layer, on Si (001) substrates [33]. In this work we demonstrate that TiN buffer layers are also adequate for the epitaxial growth of  $\text{CoFe}_2\text{O}_4$  thin films on Si (001) substrates. We further demonstrate that ion beam sputtering, IBS, is a suitable growth technique to obtain epitaxial  $\text{CoFe}_2\text{O}_4$  films. IBS has been scarcely used to grow  $\text{CoFe}_2\text{O}_4$  thin films [34], while molecular beam epitaxy (MBE) [11,13,16], pulsed laser deposition (PLD) [15,17-19,23,25-29,35] and magnetron sputtering [12,14,20-21,36] have been used frequently.

## 2. Experimental

Cobalt ferrite thin films were deposited on Si (001) substrates by ion beam sputtering. Prior to deposition, the native  $\text{SiO}_2$  was removed by dipping the substrate into a 5% HF solution for 2 min. TiN buffer layers were deposited on Si (001) by ion  $\text{Ar}^+$  sputtering from a 99.9% pure TiN target with a 3 cm Kaufmann-type ion source.  $\text{CoFe}_2\text{O}_4$  thin films were grown from two different targets: metallic  $\text{CoFe}_2$  target and  $\text{CoFe}_2\text{O}_4$  commercial target. In present work we will denote CFO\_M to the sample obtained from a pure metallic  $\text{CoFe}_2$  target and

CFO\_C to the one obtained from the  $\text{CoFe}_2\text{O}_4$  target. In both cases the CFO films have been grown in a controlled atmosphere of oxygen and argon. Both TiN buffer layers and cobalt ferrite thin films were deposited at a constant substrate temperature of  $480^\circ\text{C}$ .

The TiN/CFO bilayers were deposited in a vacuum chamber under a base pressure of  $2 \times 10^{-5}$  Pa. During deposition the pressure was maintained at  $3.3 \times 10^{-2}$  Pa and the substrates were rotated at 2 rpm to increase the homogeneity of the deposit. The same sputtering conditions, i.e. current density of sputtered atoms,  $J_{\text{sp}}$ , and energy of the sputtering  $\text{Ar}^+$  ions,  $E_{\text{sp}}$ , were kept for the TiN,  $\text{CoFe}_2$  and  $\text{CoFe}_2\text{O}_4$  targets, i.e.  $1.4 \text{ mA/cm}^2$  for  $J_{\text{sp}}$  and 600 eV for  $E_{\text{sp}}$ . The oxygen partial pressure,  $P_{\text{O}_2} = 3 \times 10^{-3}$  Pa, was also kept the same for both, CFO\_M and CFO\_C samples. After deposition, the oxygen partial pressure used during deposition was kept constant during the cooling process until the temperature was below  $150^\circ\text{C}$ .

The crystal structure and texture of the different films was analyzed by X-Ray Diffraction (XRD) in a  $\Theta/2\Theta$  configuration using a PANalytical X'Pert MPD system and Cu-K $\alpha$  radiation. Additionally  $\phi$ -scans have been performed to determine epitaxial relationships.

$^{57}\text{Fe}$  Integral Conversion Electron Mössbauer Spectroscopy (ICEMS) data were recorded at room temperature in constant acceleration mode using a  $^{57}\text{Co}(\text{Rh})$  source and a parallel plate avalanche counter [37]. The spectra were computer-fitted and the isomer shifts were referred to the centroid of the spectrum of  $\alpha\text{-Fe}$  at RT.

In-depth composition and thickness of the different layers were determined by Rutherford backscattering spectroscopy (RBS) in a 5 MV tandem accelerator using  $^4\text{He}^+$  at 1.8 MeV and 3.045 MeV. The latter energy was selected to enhance resonantly the cross section of oxygen atoms. The distribution and quantification of the various elements was determined with the SIMNRA simulation software package. RBS was also employed to estimate the thickness, included in Table 1, of the films by using a mass density of 5.20 and  $5.22 \text{ g/cm}^3$  for cobalt ferrite and titanium nitride, respectively. In addition, RBS combined with ion channeling (RBS/C) measurements were performed. A silicon barrier detector, at a scattering angle of  $170.5^\circ$ , measured the backscattering ions while a three-axis goniometer was employed to control the crystal position. Angular scans across the Si  $\langle 110 \rangle$  and  $\langle 100 \rangle$  axes were performed to determine the crystalline quality and the epitaxial relationship of the bilayer stack TiN/CFO with the silicon substrate. A combination of  $\Theta$  and tilt angle steps was used along the different axes.

X-ray photoelectron spectroscopy (XPS) data were recorded at a base pressure of  $1.5 \times 10^{-7}$  Pa using a hemispherical Phoibos 150 analyzer, Mg K $\alpha$  radiation and a constant pass energy of 20 eV.

The magnetic characterization of the bilayers was carried out in a vibrating sample magnetometer (VSM), ADE system EV7 KLA-Tencor, under a maximum magnetic field of  $\pm 18 \text{ kOe}$ , applied parallel ( $\parallel$ ) and perpendicular ( $\perp$ ) to the surface plane.

### 3. Result and Discussion

Fig. 1 shows XRD  $\Theta$ - $2\Theta$  symmetrical angular scans of the  $\text{CoFe}_2\text{O}_4$  films grown on a TiN buffer layer previously deposited on Si (001) substrates (CFO\_M and CFO\_C samples). The XRD pattern of a 70 nm TiN thin film has been included for comparison. The TiN diffraction pattern shows a main peak at  $42.76^\circ$  due to the (200) diffraction plane. In the case of the CFO/TiN bilayers, the diffraction pattern also shows a main peak at  $42.66^\circ$  and  $42.11^\circ$ , for CFO\_M and CFO\_C samples respectively. Most likely they correspond to the overlapping signals of the (400) diffraction plane of  $\text{CoFe}_2\text{O}_4$  and the (200) diffraction plane of TiN. A very narrow additional peak at  $32.99^\circ$  corresponds to the Si (200) diffraction plane of the substrate. This forbidden reflection is generally caused by multiple diffractions in  $\Theta/2\Theta$  scans [38]. The small difference between the lattice parameter of bulk  $\text{CoFe}_2\text{O}_4$  ( $a = 0.838$  nm) and twice the lattice parameter of bulk TiN ( $a = 0.424$  nm), values taken from the JCPDS cards No. 04-015-3102 and 00-038-1420 respectively, is the cause of the overlap observed between the TiN (200) and  $\text{CoFe}_2\text{O}_4$  (400) peaks in the diffractogram. In fact, the expected lattice mismatch determined by their bulk lattice spacings,  $(a_{\text{CoFe}_2\text{O}_4} - 2a_{\text{TiN}})/2a_{\text{TiN}}$ , is only -1.3%. The lattice parameters obtained for the bilayers CFO\_M and CFO\_C are 0.848 and 0.858 nm respectively, values that are larger than that of bulk cobalt ferrite. In addition these values are also larger than twice that calculated for the TiN thin film showed on Fig.1, i.e. 0.840 nm, giving rise a lattice mismatch of 1 and 2.1% for CFO\_M and CFO\_C bilayers, respectively. These results indicate an out-of-plane tensile strain that could be related with an in-plane compressive strain of the CFO thin films respect to the TiN/Si (001) substrate, especially in the case of CFO\_C bilayer. Besides, assuming that the broadening of the (400) peak is only related to grain size effects, the average crystalline domain size can be estimated using the Scherrer formula,  $d = 0.9\lambda / \text{FWHM} \cdot \cos\theta$ , where  $\lambda$  is the wavelength of the radiation used. This procedure gives values of 25 and 31 nm for CFO\_M and CFO\_C bilayers respectively. The  $\Theta/2\Theta$  scans of Fig.1 indicate that the CFO samples have a (400) out-of-plane orientation. Furthermore, the in-plane orientation was observed on Fig. 2a and 2b by  $\varphi$  scans of the (311) planes of the CFO\_M and CFO\_C bilayers respectively. No-misoriented in-plane material was observed. The presence of peaks at every  $90^\circ$  suggests a good alignment of the (001) axes of the  $\text{CoFe}_2\text{O}_4$  films and those of the TiN buffer. In order to confirm that the epitaxial relationship on both heterostructures was  $\text{CoFe}_2\text{O}_4[100]/\text{TiN}[100]/\text{Si}[100]$ ,  $\varphi$  scans of Si (111) reflections were also recorded and the results for CFO\_C sample are shown on Fig.2c. The same orientation observed for the four peaks in  $\varphi$  scans indicates that the (001) axis of the  $\text{CoFe}_2\text{O}_4$  thin film and that of silicon are parallel.

Fig. 3a and b show the random and (001) aligned spectra obtained from the RBS/C experiment with  $^4\text{He}^+$  at 1.8 MeV and a scattering angle of  $170.5^\circ$  for CFO\_M and CFO\_C samples respectively. The elemental concentrations, determined by SIMRA simulations, were also included to fit the random spectra. The fitting was done assuming a two layer model, i.e. a CFO thin film on a TiN buffer layer. The thickness

and the composition estimated from the fit were included in Table 1. They are rather similar within the experimental error ( $\approx 5\%$ ). In order to confirm the similar composition of the two bilayers, their RBS spectra were measured with a  $^4\text{He}^+$  beam of 3.045 MeV to enhance the oxygen signal (Fig.3c). The main difference between both spectra arises from the different TiN thickness, 4 and 9 nm for CFO\_M and CFO\_C samples respectively.

When Rutherford spectroscopy is performed in a channeling configuration, i.e. when the ion beam is directed along a major crystal axis of the films and substrate, the effective density of atoms seen by the particle beam is reduced because surface atoms shadow deeper atoms and a reduced backscattering yield is consequently observed. In fact, RBS/C can be used to explore the crystalline quality of thin films and their epitaxial relationship with the substrates. The ratios of the backscattering yield along (001) to that in a random direction for the Fe+Co atoms of the CFO\_M and CFO\_C bilayers are  $\chi_{\min}(\text{Fe+Co}) \approx 65\%$  and  $70\%$ , respectively, near the surface. These ratios increase at lower channel numbers indicating a higher defect density at the  $\text{CoFe}_2\text{O}_4/\text{TiN}$  interface. The loss of channeling at the interface has also been observed in other thin film materials such as  $\text{SrTiO}_3$  deposited on  $\text{TiN}/\text{Si}(100)$  substrates [39] or  $\text{Fe}_3\text{O}_4$  deposited on different single crystal oxide substrates [40,41]. In order to compare both samples we have plotted on Fig. 3d their channeling spectra corresponding to the Fe+Co atoms. Even both samples show a reduced degree of channeling at the interface, the effect is more important for the CFO\_M bilayer, in which a clear step appears in the spectrum.

In both samples, CFO\_M and CFO\_C, the yield value for silicon atoms is  $\chi_{\min}(\text{Si}) \approx 60\%$  and there is almost no channeling observed on Ti atoms from the TiN buffer layer. The  $\chi_{\min}$  values of Si and Fe+Co signals are relatively larger when compared with those reported for other spinel oxide films such as magnetite grown on single crystal MgO substrates ( $\chi_{\min}(\text{Fe}) \approx 22\text{-}30\%$  [40,41]). However, in our case the alignment of the  $\text{CoFe}_2\text{O}_4$  thin film with the Si (001) substrate takes place through a domain matching epitaxy instead of a lattice matching epitaxy. In addition, even though the TiN thickness (4 – 9 nm) is enough to align the  $\text{CoFe}_2\text{O}_4$  thin film with the Si (001) substrate, the absence of channeling yield for the Ti atoms could indicate that the thickness of the TiN buffer is not enough to obtain a well-ordered TiN layer on the Si (001) substrate. Therefore, interface effects dominate the RBS/C spectra.

The angular scans of the scattering yield of Fe+Co atoms and Si atoms from the substrate were measured along the  $\langle 100 \rangle$  and  $\langle 110 \rangle$  directions to examine the axis relationship between the  $\text{CoFe}_2\text{O}_4$  and the Si. Fig. 4a and Fig. 4b show the experimental  $\langle 110 \rangle$  and  $\langle 100 \rangle$  scans for the CFO\_M bilayer and Fig. 4c and Fig. 4d the corresponding ones for the CFO\_C bilayer. The normalized yields are obtained as the backscattering yield at each value of the tilt angle divided by that obtained in a random geometry. It can be observed that both CFO films exhibit a relatively good channeling along the  $\langle 100 \rangle$  and  $\langle 110 \rangle$  directions and that the channeling directions of the  $\text{CoFe}_2\text{O}_4$  films and the corresponding ones of the silicon substrates are very similar since the channeling dips of Fe+Co atoms are well aligned respect to the silicon ones.

Only a small channeling dip shift of  $\approx 0.1^\circ$  of Fe+Co respect to Si can be detected in both samples along the  $\langle 110 \rangle$  direction. These results confirm the epitaxial relationship of the  $\text{CoFe}_2\text{O}_4$  thin films with the TiN buffer Si (001) substrate.

The magnetic properties of cobalt ferrite thin films depend mainly on the Fe and Co cation distribution. We have used two techniques, XPS and Mössbauer spectroscopy, to glean this information. The Co 2p, Fe 2p and O 1s core-level spectra for CFO\_M and CFO\_C bilayers are shown on Fig. 5a, 5b and 5c respectively. First we point out the strong similarities between both samples for the three core level spectra. The main components of the Co2p spectra are two asymmetrical peaks corresponding to the  $2p_{3/2}$  and  $2p_{1/2}$  core levels at 780.1 and 795.7 eV, respectively, and the shake-up satellites at binding energies of 786.2 and 802.5 eV. The presence of strong satellites is characteristic of  $\text{Co}^{2+}$ . The quantitative peak fitting procedure for Co2p is rather complicate. Zhou et al. [42] fitted the  $2p_{3/2}$  peak in terms of two symmetrical contributions due to  $\text{Co}^{2+}$  ions in octahedral and tetrahedral sites. However, since it is not possible to discard an asymmetrical line-shape for the  $2p_{3/2}$  and  $2p_{1/2}$  levels due to the presence of unresolved multiplet splitting, this kind of analysis has some uncertainties. In any case, assuming an analysis in terms of six symmetrical contributions (show on Fig. 5a for the CFO\_C sample), two for the  $2p_{3/2}$  level at binding energies of 780.0 and 782.3 eV, two for the  $2p_{1/2}$  level at binding energies of 795.7 and 797.8 eV and two for the corresponding satellites, we obtain an estimate of 75%  $\text{Co}^{2+}$  cations in octahedral sites.

The Fe2p spectra are composed by a spin-orbit doublet with main peaks at binding energies of 710.7 and 724.2 eV for the  $2p_{3/2}$  and  $2p_{1/2}$  core levels, respectively, plus a small satellite around 718 eV. The binding energies of the main photoemission peaks and the satellite are characteristic of  $\text{Fe}^{3+}$ . The main photoemission peaks are quite broad and its quantifications in terms of  $\text{Fe}^{3+}$  in octahedral and tetrahedral sites is really quite complex. The very well-known existence of unresolved multiplet splitting can affect strongly the final result.

The O1s spectra of both bilayers have been fitted in terms of three symmetrical peaks at 529.9, 531.3 and 532.4 eV which we associate to oxygen in the oxygen lattice bonded to Fe and Co, surface hydroxyl (Fe and Co bonded to OH) and absorbed  $\text{H}_2\text{O}$  at the surface, respectively [36]. The binding energies of the different contributions appear at the same position for both bilayers and the contribution of the oxygen at the lattice accounts  $\approx 80\%$  of the total O 1s area.

Fig. 6a and 6b show the transmission Mössbauer spectra recorded at RT and 26 K from the commercial  $\text{CoFe}_2\text{O}_4$  target used for the deposition of the CFO\_C bilayer. The asymmetry of the highest velocity peak suggests the presence of at least two different contributions which are more evident in the 26 K spectrum. Thus, both spectra were fitted with two sextets, corresponding to  $\text{Fe}^{3+}$  in tetrahedral (A) and octahedral (B) sites. The corresponding Mössbauer parameters are collected on Table 2. The area ratio between A and B components at in the 26 K spectrum is 1.2, close to the expected value for a completely inverse stoichiometric cobalt ferrite  $(\text{Fe}^{3+})_A(\text{Co}^{2+}\text{Fe}^{3+})_B\text{O}_4$ , that should be 1. However, at RT spectrum, the area ratio

between A and B component is 1.8. This result has been observed in other spinel oxides and it has explained by an increasing overlap of the A and B site Zeeman patterns with temperature [43]. The origin of the overlap is a supertransferred hyperfine field between A and B sites. A significant part of the B-site  $\text{Fe}^{3+}$  ions feel hyperfine fields close to the average field acting on A sites and the A-site spectral area result overestimated [43].

The Mössbauer spectra from CFO\_C and CFO\_M bilayers are shown on Fig. 6c and 6d respectively. The spectra have been fitted with two sextets and the Mössbauer parameters are included in Table 2. We have used similar isomer shifts than that obtained from the target spectrum for the tetrahedral and octahedral  $\text{Fe}^{3+}$  ions and we have also fixed the same width for the two sextet components. Sample CFO\_M shows for the  $\text{Fe}_\text{A}^{3+}$  A-site sextet a hyperfine magnetic field of  $H_\text{hyp} = 47.2$  T while for the  $\text{Fe}_\text{B}^{3+}$  B-site the hyperfine magnetic field is 49.4 T. In the case of the CFO\_C sample the hyperfine magnetic fields for the  $\text{Fe}_\text{A}^{3+}$  A-site sextet and  $\text{Fe}_\text{B}^{3+}$  B-site are 49.0 and 51.8 T respectively, slightly higher than those of the target. The central part of the spectra has additional contributions that can be fitted in terms of a doublet and a singlet compatible with the presence of  $\text{Fe}_{1-x}\text{O}$  that could be present at the surfaces and interfaces. The calculated A/B ratio is similar to that shown in the RT spectrum of the target if we take into account the errors due to the overlap between A and B Zeeman patterns.

Important information about the magnetic anisotropy can be derived from the analysis of the relative intensities of the Zeeman sextets. The relative line intensity of a magnetically split sextet is  $3 : x : 1 : 1 : x : 3$ . The x value depends on the angle between the incident  $\gamma$ -rays and the hyperfine field. When the  $\gamma$ -rays impinge perpendicularly on the sample surface, the x values may change from 0 (magnetization perpendicular to the film surface) to 4 (magnetization in-plane). The value that gives us a better fit for the target Mössbauer spectra is 2, which corresponds most likely to a random orientation of the magnetization. In the case of both bilayers the best fit is obtained with an x value of 4 indicating an in-plane magnetization.

The hysteresis loops of CFO\_M and CFO\_C bilayers measured at room temperature are plotted on Fig. 7a and 7b respectively. We have subtracted the diamagnetic component from the raw M-H hysteresis curve by using the measurements of a silicon sample with the same volume of CFO\_M and CFO\_C samples. The measurements were performed with the magnetic field applied in-plane (along a Si  $\langle 110 \rangle$  direction) and out-of-plane. We cannot reach saturation at the maximum magnetic field of our setup, 18 KOe, however it is possible to establish some points about the magnetic behavior of the samples. In both samples, CFO\_M and CFO\_C, the remanent magnetization and the coercivity take significantly larger values for the in-plane hysteresis loops indicating that the magnetization easy axis is mainly parallel to sample surface. The in-plane hysteresis loops of CFO\_M and CFO\_C bilayer show a double step-structure. In the case of CFO\_C bilayer, a small drop around zero fields is observed. This feature at low fields has been reported by other authors [11,13,20,21,23]. Rigato et al. [21] observed that the M-H loop become sheared as thickness was increased. They have found a



microscopic origin of this anomalous behavior that depends on surface microstructure and results from the balance of the different energy contributions during the film growth. Jin et al. [20] have attributed the two step to two magnetic phases, one to the bulk and the other close to the surfaces and interfaces. In the case of CFO\_M the double-step structure is clearly observed. However the low field step is not close to zero field and appears at 1.4 KOe. We note that, neither, XPS or XRD, give any indication of the presence of two phases. However, the shape of the channeling spectrum (Fig. 3d) reveals that we cannot disregard the presence of a second additional phase in this sample, one of them induced at the interface with TiN at the beginning of the CoFe<sub>2</sub>O<sub>4</sub> deposition process.

The in-plane magnetization at the maximum field, 18 KOe, is  $\approx 200 \text{ emu/cm}^3$  for both bilayers, which is clearly below the magnetization saturation of the CoFe<sub>2</sub>O<sub>4</sub> bulk,  $400 \text{ emu/cm}^3$ . The M-H hysteresis loops of CFO samples are clearly unsaturated so we expect a saturation magnetization higher than  $200 \text{ emu/cm}^3$ . In any case, a reduced magnetization is a common issue on CoFe<sub>2</sub>O<sub>4</sub> thin films deposited on different substrates and buffer layers [13,16,20,21,23,35] and is usually attributed to grow defects as antiphase boundaries [13], strains [16], partial spinel crystal structure [16], structure defects in the un-continuous top layers [20] or to misfit dislocations at the interface [15]. In addition, it has been shown to depend on film thickness [20,21].

The CFO\_M and CFO\_C samples show magnetic anisotropy between in-plane and out-of-plane directions. The coercive field, included on Table 1, when the field is applied along the in-plane direction for CFO\_M sample is 460 mT, larger than that for the out-of-plane direction, 200 mT. The difference between in-plane and out-of-plane coercive fields is higher for the CFO\_C sample (475 and 76 mT respectively). These results and the shape of in-plane and out-of-plane M-H loops indicate that the magnetization of the CFO\_C sample lies completely in the sample surface. In the case of CFO\_M sample an out-of-plane magnetization component could be present.

Similar behavior, with an easy-magnetization in-plane, has been found in epitaxial CFO films grown in-plane compressively strained on SrTiO<sub>3</sub> (001) [19,20,21] or MgAl<sub>2</sub>O<sub>4</sub> (001) [11] substrates. On the contrary, an easy-axis perpendicular to the surface plane is generally found when CFO grows under in-plane tensile strain, as for example on MgO (001) substrates [13] or on Si (100) buffer with a MgO layer [23]. In our case, the large in-plane magnetic anisotropy observed on CFO\_C sample can be related to the in-plane compressive strain induced in the CFO thin films by the presence of the TiN buffer layer. This explanation is supported by the XRD data that indicate the presence of in-plane compressive strains, stronger in CFO\_C sample.

The origin of the different strain found in CFO thin films in CFO\_M and CFO\_C samples, one grown with a metallic target and the other with an oxide ceramic one, may be related to the different sputtering processes that are taking place during the growth. It is well known that reactive sputtering of a metallic target can be done in metal and in oxide mode [43]. In metal mode, a high deposition rate and poor stoichiometry are generally found and the optimum deposition conditions are obtained in the transition between both modes. In magnetron sputtering processes, the presence of energetic

negative oxygen ions that are generated via sputtering of the oxide region of the target, is well established. Tominaga et al. [44] have found that its amount increases as the oxide layer at the target gets thicker. In the case of a metallic target, the presence of energetic negative oxygen ions depends on the partial pressure and the oxidation of the metal target while for oxide ceramic targets, the target surface is always an oxide, and thus a higher amount of energetic oxygen is expected. The presence of energetic oxygen ions in the sputtering process is an important factor to control the crystal structure of the growing film [45,46] as it has been observed on ZnO films that develop an unusual (11 $\bar{2}$ 0) orientation in oxide mode reactive sputtering [46]. The energetic oxygen ions, generated at that target, easily bombard the substrate during the deposition under low gas pressure where the mean free path is long. Since in our sputtering process we use the same oxygen partial pressure and total pressure for the sputtering of both targets (i.e. metallic and insulator), we expect a higher amount of energetic oxygen ions inducing structural effects in the substrates in the case of the ceramic target, that explain the larger in-plane compressive strains observed on the CFO\_C sample.

#### **4. Conclusions**

Epitaxial CoFe<sub>2</sub>O<sub>4</sub> thin films have been grown on TiN buffer Si (001) substrates by ion beam sputtering by using ceramic or metallic targets. The epitaxial relationship is CoFe<sub>2</sub>O<sub>4</sub> [100] / TiN [100] / Si [100] as shown by XRD and RBS\_channeling measurements. In-plane magnetic anisotropy is detected and attributed to the in-plane compressive strain induced by the TiN buffer layer, which is further enhanced in CoFe<sub>2</sub>O<sub>4</sub> thin films grown from a ceramic target. We have thus demonstrated that should be possible to integrate CoFe<sub>2</sub>O<sub>4</sub> thin films on silicon based devices by using TiN buffer layers. Ion beam sputtering is a suitable technique to obtain epitaxial CoFe<sub>2</sub>O<sub>4</sub> thin films on silicon substrates. Our results might light the role of reactive sputtering processes that take place on metal or insulator oxide targets allowing a fine control of the magnetic anisotropy.

#### **Acknowledgments**

This work was supported by the Spanish Ministry of Economy under the project number MAT2015-64110-CO2.

## References

- [1] Y. K. Takahashi, S. Kasai, T. Furubayashi, S. Mitani, K. Inomata and K. Hono, *Appl. Phys. Lett.* 96 (2010) 072512.
- [2] Q. Dai, D. Berman, K. Virwani, J. Frommer, P-O. Jubert, M. Lam, T. Topuria, W. Imaino and A. Nelson, *Nano Lett.*, 10 (2010) 3216-3221.
- [3] D. Erdem, N. S. Bingham, F. J. Heiligt, N. Pilet, P. Warnicke, L. J. Heyderman and M. Niederberger, *Adv. Funct. Mater.* 26 (2016) 1954-1963.
- [4] *Handbook of Magnetism and Advanced Magnetic Materials*, Wiley-Blackwell, 2007.
- [5] S. A. Chambers, R. F. C. Farrow, S. Maat, M. F. Toney, L. Folks, J. G. Catalano, T. P. Trinor and G. E. Brown, *J. Magn. Magn. Mater.* 246 (2002) 124-139.
- [6] J. H. Park, J-H. Lee, M. G. Kim, Y. K. Jeong, M-A. Oak, H. M. Jang, H. J. Choi and J. F. Scott, *Phys. Rev. B* 81 (2010) 134401.
- [7] D. Peddis, N. Yaacoub, M. Ferretti, A. Martinelli, G. Piccaluga, A. Musinu, C. Cannas, G. Navarra, J. M. Greneche and D. Fiorani, *J. Phys.: Condens. Matter* 23 (2011) 426004.
- [8] V. Rusanov, V. Gushterov, S. Nikolov and A. X. Trautwein, *Hyperfine Interact.* 191 (2009) 67-74.
- [9] S. J. Kim, W. Lee W and C. S. Kim, *Jpn. J. Appl. Phys.* 40 (2001) 4897-4902.
- [10] J.C. Slonczewski, *Phys. Rev.* 19 (1958) 1341-1348.
- [11] S. Matzen, J.-B. Moussy, R. Mattana, F. Petroff, C. Gatel, B. Warot-Fonrose, J. C. Cezar, A. Barbier, M.-A. Arrio and Ph. Sainctavit, *Appl. Phys. Lett.* 99 (2011) 052514.
- [12] T. Niizeki, Y. Utsumi, R. Aoyama, H. Yanagihara, J. Inoue, Y. Yamasaki, H. Nakao, K. Koike and E. Kita, *Appl. Phys. Lett.* 103 (2013) 162407.
- [13] H. Yanagihara, K. Uwabo, M. Minagawa, E. Kita and N. Hirota, *J. Appl. Phys.* 109 (2011) 07CC122.
- [14] H. Yanagihara, M. Oka, Y. Utsumi, T. Niizeki, K. Z. Suzuki K.Z, J.-I. Inoue and E. Kita, *IEEE Trans. Magn.* 50 (2014) 2102904.
- [15] A.-K. Axelsson, F. Aguesse, V. Tileli, M. Valant and N. M. Alford, *J. Alloys Compd.* 578 (2013) 286.
- [16] J. A. Moyer, D. P. Kumah, C. A. F. Vaz, D. A. Arena and V. E. Henrich, *J. Magn. Magn. Mater.* 345 (2013) 180-189.
- [17] J. de la Figuera, A. Quesada, L. Martín-García, M. Sanz, M. Ouja, E. Rebollar, M. Castillejo, P. Prieto, A. Muñoz-Martín, L. Aballe and J. F. Marco, *Appl. Surf. Sci.* 359 (2015) 480-485.
- [18] J. de la Figuera, A. Quesada, L. Martín-García, M. Sanz, M. Ouja, M. Castillejo, A. Mascaraque, A. T. N'Diaye, M. Foerster, L. Aballe and J. F. Marco, *Croat. Chem. Acta*, 2015, 88(4), 453-460.
- [19] P. D. Thang, G. Rijnders and D. H. A. Blank, *J. Magn. Magn. Mater.* 310 (2007) 2621.
- [20] C. Jin, H. Liu, P. Li, D. F. Kuang and H. L. Bai, *J. Appl. Phys.* 110 (2011) 013917.
- [21] F. Rigato, J. Geshev, V. Skumryev and J. Fontcuberta, *J. Appl. Phys.* 106 (2009) 113924.
- [22] S. R. Singamaneni, J. T. Prater and J. Narayan, *Appl. Phys. Rev.* 3 (2016) 031301.

- [23] M. Ning, J. Li, C. K. Ong and S. J. Wang, *J. Appl. Phys.* 103 (2008) 013911.
- [24] N. T. H. Kim-Ngan, A. G. Balogh, J. D. Meyer, J. Brötz, M. Zajac, T. Slezak and J. Korecki, *Surf. Sci.* 603 (2009) 1175-1181.
- [25] K. A. Shaw, E. Lochner and D. M. Lind, *J. Appl. Phys.* 87 (2000) 1727-1733.
- [26] R. Bachelet, P. de Cous, B. Warot-Fonrose, V. Skumryev, J. Fontcuberta and F. Sánchez, *J. Appl. Phys.* 110 (2011) 086102.
- [27] R. Bachelet, P. de Caux, B. Warot-Fonrose, V. Skumryev, J. Fontcuberta and F. Sánchez, *Thin Solid Films* 519 (2011) 5726-5729.
- [28] F. Sánchez, R. Bachelet, P. de Caux, B. Warot-Fonrose, V. Skumryev, L. Tarnawska, P. Zaumseil, T. Schroeder and J. Fontcuberta, *Appl. Phys. Lett.* 99 (2011) 211910.
- [29] X. S. Gao, D. H. Bao, B. Birajdar, T. Habisreuther, R. Mattheis, M. A. Schubert, M. Alexe and D. Hesse, *J. Phys. D: Appl. Phys.* 42 (2009) 175006.
- [30] J. Narayan and C. Larson, *J. Appl. Phys.* 93 (2003) 278-285.
- [31] P. R. Willmott, R. Timm and J. R. Huber, *Appl. Surf. Sci.* 127 (1998) 105-110.
- [32] R. Chowdhury, X. Chen X and J. Narayan, *Appl. Phys. Lett.* 64 (1994) 1236-1238.
- [33] P. Prieto, J. de la Figuera, L. Martin-Garcia, J. E. Prieto and J. F. Marco, *J. Mater. Chem. C* 4 (2016) 7632-7639.
- [34] S. Schnittger, C. Jooss, S. Sievers, *Journal of Physics: Conference Series* 200 (2009) 072086.
- [35] M. Khodaei, S. A. S. Ebrahimi, Y. J. Park, J. M. Ok, J. S. Kim, J. Son and S. Baik, *J. Magn. Magn. Mater.* 340 (2013) 16-22.
- [36] S. E. Shirsath, X. Liu X, Y. Yasukawa, S. Li and A. Morisako, *Scientific reports*, 6:30074, DOI:10.1038/srep30074.
- [37] R. Gancedo, M. Gracia and J. F. Marco, *Hyperfine Interact.* 66 (1991) 83-94.
- [38] P. Zaumseil, *J. Appl. Cryst.* 48 (2015) 528-532.
- [39] R. D. Vispute, J. Narayan, K. Dovidenko, K. Jagannadham, N. Parikh, A. Suvkhanov and J. D. Budai, *J. Appl. Phys.* 80(12) (1996) 6720-6724.
- [40] P. Prieto, J. E. Prieto, R. Gargallo-Caballero, J. F. Marco and J. de la Figuera, *Appl. Surf. Sci.* 359 (2015) 742-748.
- [41] N. T. H. Kim-Ngan, A. G. Balogh, J. D. Meyer, J. Brötz, S. Hummelt, M. Zajac, T. Slezak and J. L. Korecki, *Surf. Sci.* 602 (2008) 2358-2362.
- [42] Z. Zhou, Y. Zhang, Z. Wang, W. Wei, W. Tang, J. Shi and R. Xiong, *Appl. Surf. Sci.* 254 (2008) 6972-6975.
- [43] R.E. Vandenberghe and E. De Grave in G.J. Long and J. Grandjean (Eds), *Mossbauer Spectroscopy Applied to Inorganic Chemistry*, Springer Science + Business Media, 1989, p. 74 and 102.
- [44] K. Tominaga, T. Kikuma, K. Kusaka and T. Hanabusa, *Vacuum* 66 (2002) 279-284.
- [45] S. Mráz and J. M. Schneider, *J. Appl. Phys.* 100 (2006) 023503.
- [46] S. Takayanagi, T. Yanagitani and M. Matsukawa, *J. Cryst. Growth* 363 (2013) 22-24.

## Figure Captions

**Fig.1** X-ray diffraction patterns of CFO\_M and CFO\_C bilayers and a TiN thin film in  $\Theta/2\Theta$  configuration.

**Fig. 2**  $\varphi$  scans around  $\text{CoFe}_2\text{O}_4$  (311) reflection for CFO\_M (a) and CFO\_C (b) bilayers. c)  $\varphi$  scan around Si (111) reflection.

**Fig. 3** (a) and (b) Random RBS spectra of CFO\_M and CFO\_C bilayers obtained with  $^4\text{He}^+$  ions at 1.8 MeV and its simulation. The surface energies for Fe, Co, Ti, Si and O are indicated by arrows. The RBS (001) aligned spectra have also included (red circles). (c) RBS spectra of CFO\_M and CFO\_C bilayers obtained with  $^4\text{He}^+$  ions at 3.045 MeV. (d) RBS (001) aligned spectra corresponding to Fe+Co atoms of CFO\_M and CFO\_C bilayers for comparison.

**Fig. 4** Channeling scans for Si and Fe+Co atoms along  $\langle 110 \rangle$  (a and c) and  $\langle 100 \rangle$  (b and d) directions for CFO\_M and CFO\_C bilayers respectively.

**Fig. 5** (a), (b) and (c), Co2p, Fe 2p and O1s core level spectra for CFO\_M and CFO\_C bilayers as labelled.

**Fig. 6** Room temperature (a) and 26 K (b) ICEMS Mössbauer spectra recorded from  $\text{CoFe}_2\text{O}_4$  commercial target and (c) and (d) for CFO\_C and CFO\_M bilayers respectively. The corresponding fits, whose parameters are shown in Table 2, are also included.

**Fig 7** Magnetization loops at room temperature for (a) CFO\_M and (b) CFO\_bilayers with the magnetic field applied parallel and perpendicular to the film plane.

**Table 1.** Lattice constant, a, RBS thickness and composition and in-plane and out-of-plane coercive fields for CFO\_M and CFO\_C bilayers.

Sample	a (nm)	Thickness TiN/CFO (nm)	Co/ Fe/ O	H <sub>c</sub> in-plane (mT)	H <sub>c</sub> out-plane (mT)
CFO_M	0.848	4 / 94	1/1.9 / 3.9	460	200
CFO_C	0.858	9/ 91	1/1.9 / 4.1	475	76

Table 2

**Table 2.** Mössbauer fit parameters for the CFO target at RT and 26 K and for the CFO samples at RT.

	IS (mm/s)	$2\epsilon/\Delta$ (mm/s)	$H_{\text{hyp}}$ (T)	Area (%)
<b>Target_RT</b>				
Sextet $\text{Fe}_A^{3+}$	0.29	0.01	48.5	64.7
Sextet $\text{Fe}_B^{3+}$	0.36	-0.07	51.1	35.3
<b>Target_26 K</b>				
Sextet $\text{Fe}_A^{3+}$	0.40	-0.02	51.5	51.1
Sextet $\text{Fe}_B^{3+}$	0.51	-0.06	54.3	41.0
<b>CFO_M (RT)</b>				
Sextet $\text{Fe}_A^{3+}$	0.29	0.06	47.2	65.6
Sextet $\text{Fe}_B^{3+}$	0.36	-0.09	49.4	27.4
Singlet $\text{Fe}_{1-x}\text{O}$	1.49	---	---	3.3
Doublet $\text{Fe}_{1-x}\text{O}$	-0.03	0.96	---	3.6
<b>CFO_C (RT)</b>				
Sextet $\text{Fe}_A^{3+}$	0.29	0.02	49.0	60.8
Sextet $\text{Fe}_B^{3+}$	0.37	-0.01	51.8	34.8
Singlet $\text{Fe}_{1-x}\text{O}$	1.51	---	---	1.8
Doublet $\text{Fe}_{1-x}\text{O}$	-0.46	1.02	---	2.5

Fig.1

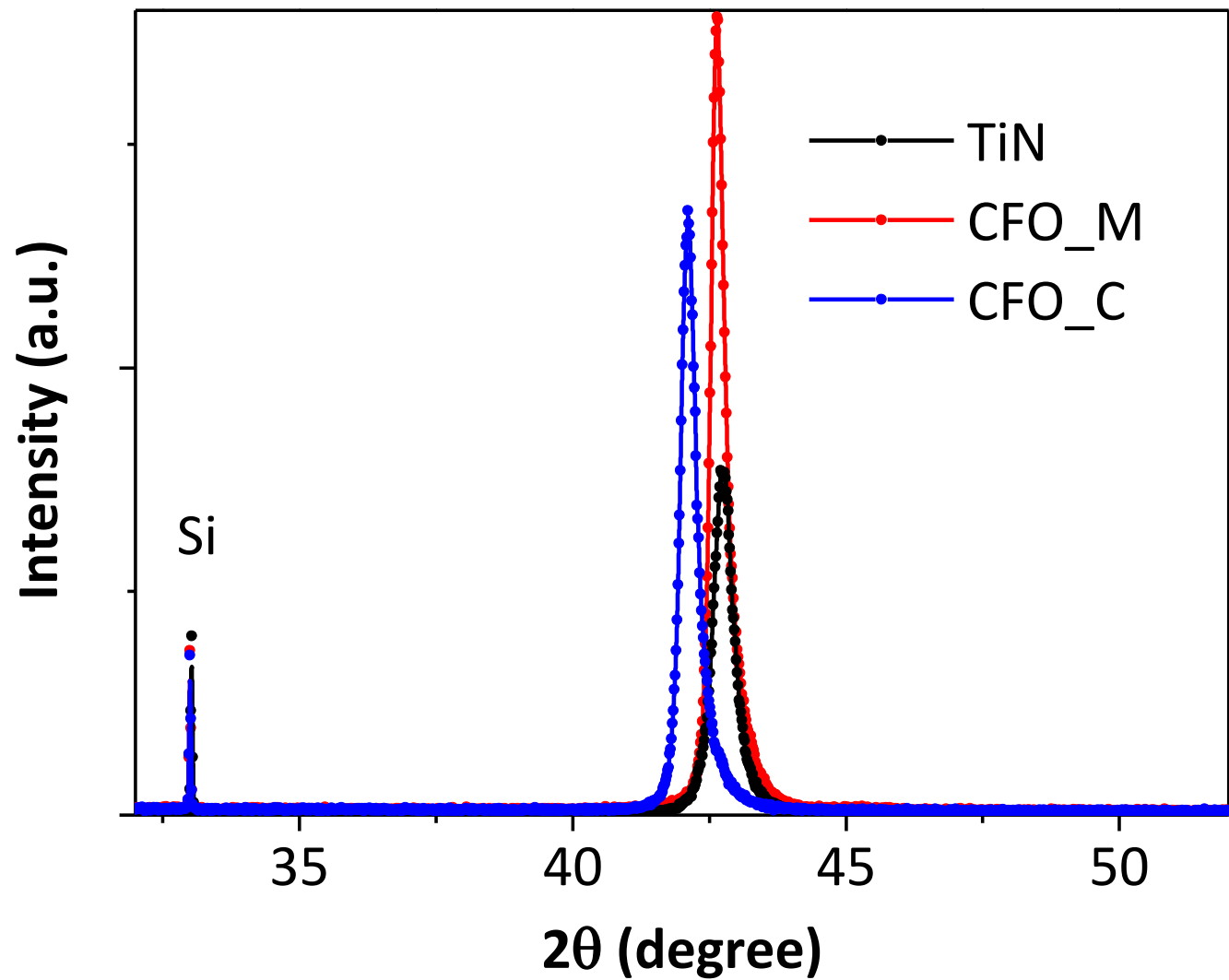




Fig.2

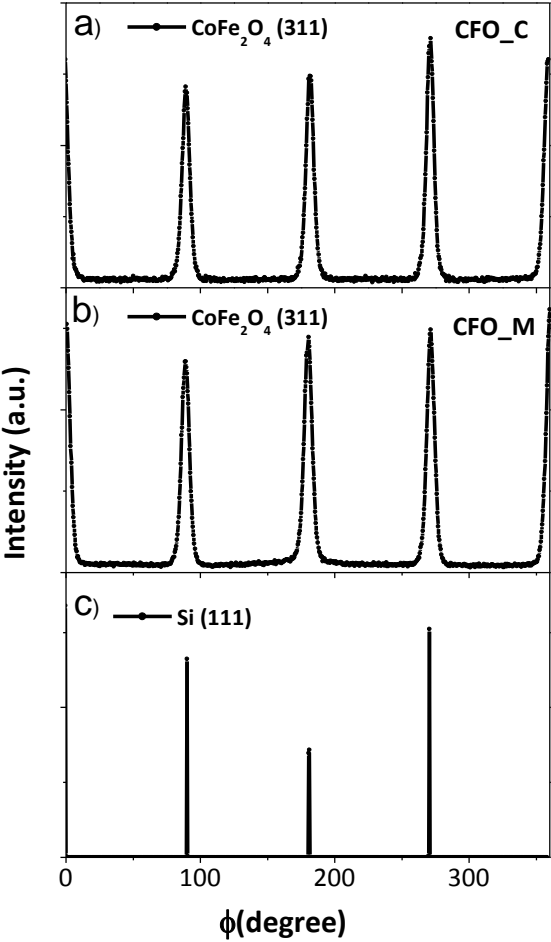


Figure 3  
[Click here to download Figure: Figure\\_3\\_referees.pptx](#)

Fig.3

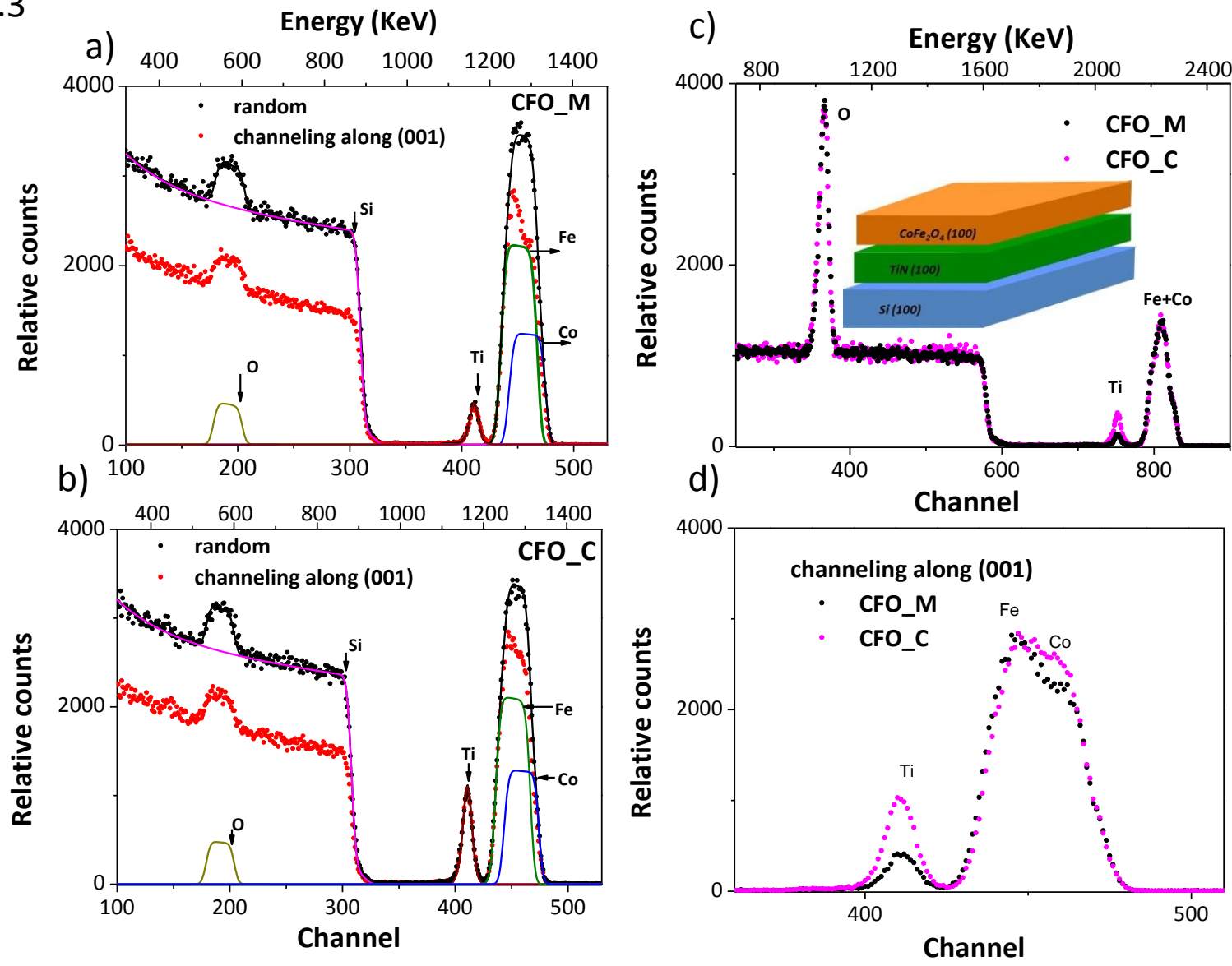


Figure 4  
[Click here to download Figure: Figure\\_4.pptx](#)

Fig.4

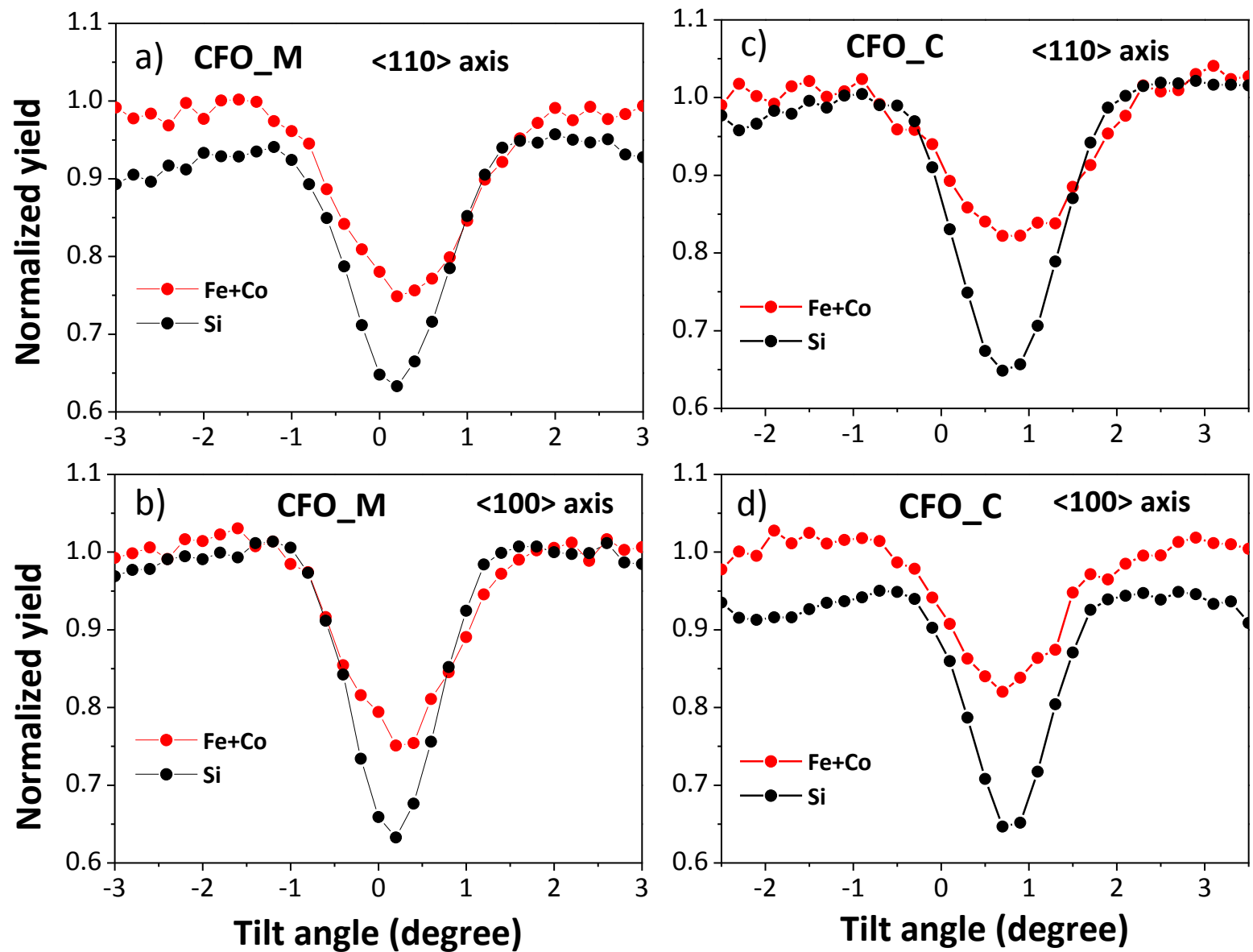


Figure 5  
Click here to download Figure: Figure\_5\_referres\_vertical.pptx

Fig.5

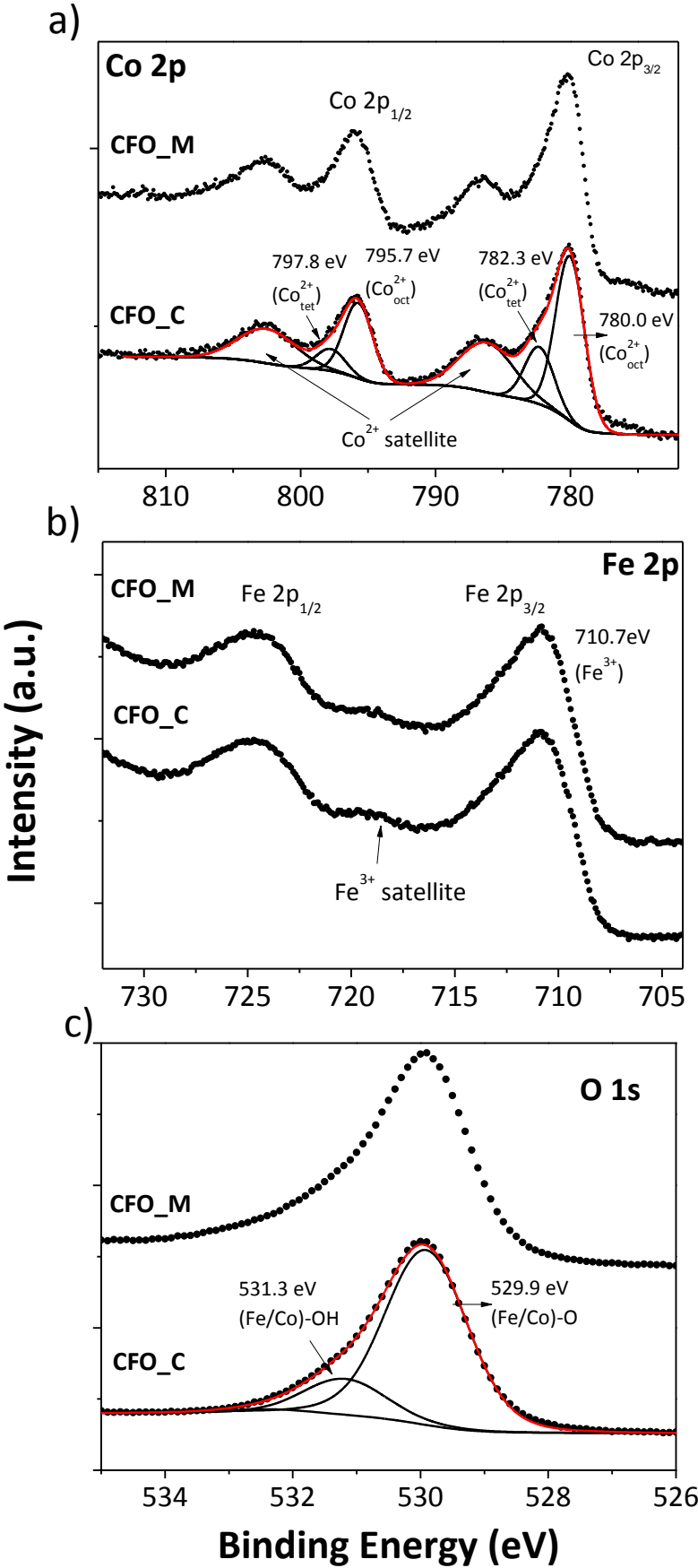


Fig.6

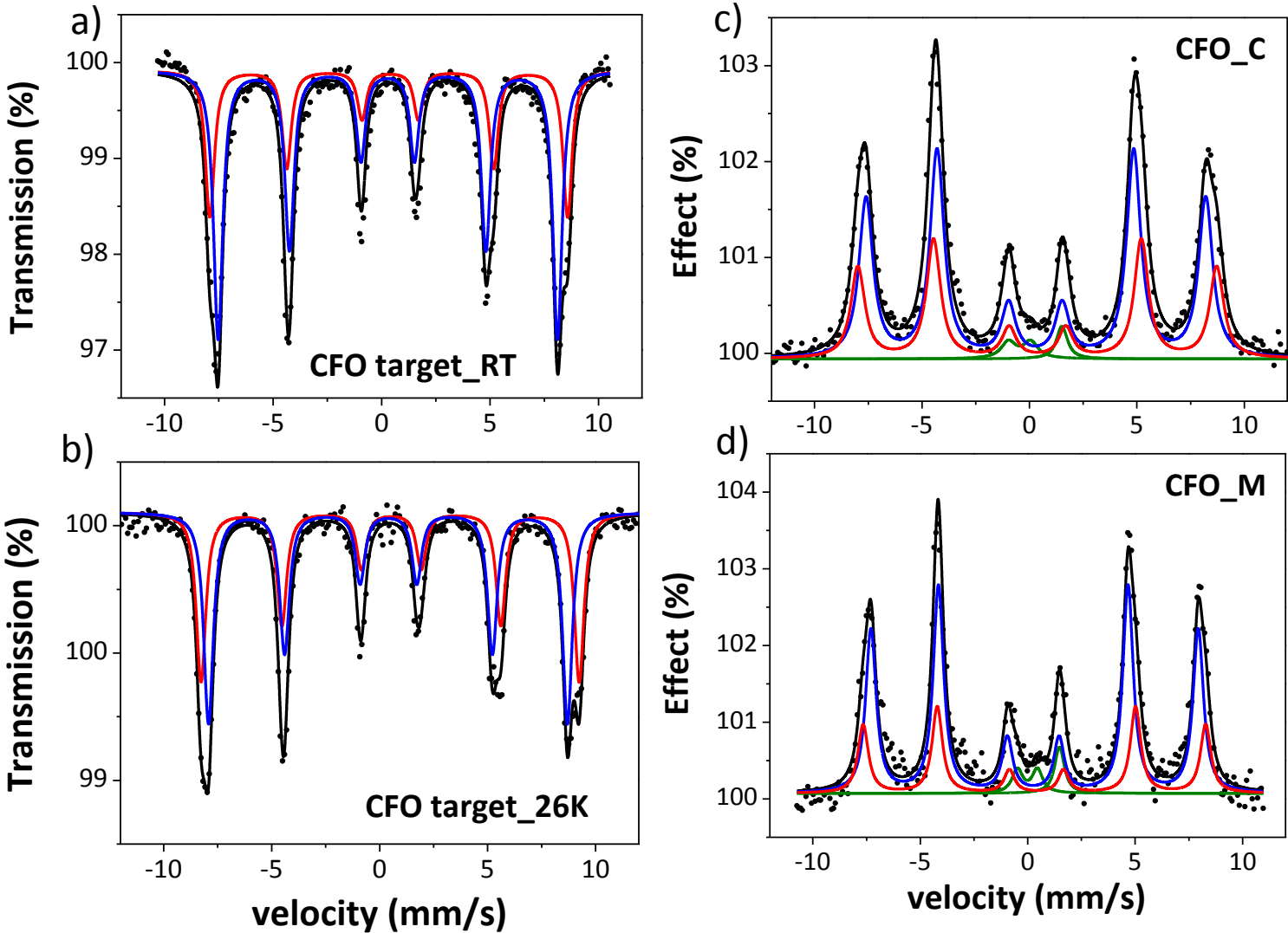


Figure 7  
Click here to download Figure: Figure\_7\_referees.pptx

